21.4 A 263 GHz 32-channel EPR-on-a-chip injection-locked VCO-array

Anh Chu*[1], Michal Kern*[1], Khubaib Khan[1], Klaus Lips[2], Jens Anders[1,3]

[1]University of Stuttgart, Stuttgart, Germany, [2]Helmholtz-Zentrum Berlin für Materialien und Energie, Berlin, Germany, [3]Institute for Microelectronics Stuttgart, (IMS CHIPS), Stuttgart, Germany

Electron paramagnetic resonance (EPR) spectroscopy is a powerful technique that uses the spin of an unpaired electron as a nanoscopic probe inside a molecule to extract information about its chemical structure and composition as well as its surroundings via small changes in its resonance frequency, see Fig. 21.4.1 (left). EPR has applications in studying and monitoring a wide range of materials, starting from defects in semiconductors over free radicals in the blood to metal catalysts in hydrogen fuel production. EPR measurements are typically performed in moderate static magnetic fields around 0.3 T, corresponding to EPR frequencies around 9 GHz. This combination of field and frequency is commonly used due to the relative ease of generation of 0.3 T magnetic fields with sufficient homogeneity as well as the required 9 GHz frequency signal. However, access to higher frequencies and fields is strongly desirable due to higher spin polarization (with corresponding increased signal amplitude), higher spectral resolution, which allows, e.g., the determination of electronic and geometric structures of active centers in enzymes, and access to higher energy electronic transitions, such as those found in metal complexes or materials interesting for antiferromagnetic spintronics, explaining the ongoing research towards high-frequency EPR (HFEPR) with operating frequencies beyond 90 GHz. Here, another strong driver of HFEPR is the field of dynamic nuclear polarization (DNP), a method that can be used to boost the relatively poor sensitivity of nuclear magnetic resonance (NMR) by transferring the intrinsically higher electron polarization to the nuclear spins. Today, there are only a few commercial HFEPR-based DNP spectrometers on the market, with the most popular ones operating at an EPR frequency of 263 GHz (9.4 T), corresponding to a proton NMR frequency of 400 MHz. This instrument uses a gyrotron as its source for the mm-wave magnetic field (B_1 field) and costs far beyond 1 Mio. €.

Current HFEPR spectrometers use one of four methods to generate B_1-fields for HFEPR/DNP: vacuum tubes (gyrotrons and backward-wave oscillators), active frequency multiplier chains, synchrotron radiation, and, most recently, THz photomixers. All these methods, however, have significant drawbacks regarding their complexity and costs: the first three methods have to use large (>1 m^2), complex quasi-optical setups to efficiently manipulate the mm-wave beam and use cryogenically cooled radiation detectors (bolometers) for sensitive detection. THz photomixers need only a few THz lenses but require complex optical fiber equipment to achieve sufficient spectral resolution and lack the sensitivity of the other methods.

To overcome the limitations of conventional EPR setups, over the last decade, several oscillator-based CMOS-integrated EPR detectors (EPR-on-a-chip) were presented at various fundamental frequencies up to 146 GHz [1]. Here, a single HFEPR oscillator operating at 90 GHz was also used to measure EPR at 360 GHz by exploiting its fourth harmonic, however, with significantly lower excitation power and sensitivity. With the small coil diameter of 45 µm for the 146 GHz oscillator imposed by the wavelength of the fundamental frequency, the single-coil, standard LC tank VCO approach in [1] cannot be effectively used for EPR and DNP experiments at very high operating frequencies. In [2], the use of injection-locked VCO arrays has been proposed as an efficient means both for increasing the lateral sensitivity volume and, at the same time, lowering the phase noise, see Fig. 21.4.1 (right). Here, we propose to use electrically large inductors, i.e., inductors whose perimeter is a significant fraction of the wavelength, as tank inductors inside arrays of injection-locked VCO-based EPR detectors to significantly extend the sensitive volume in the direction perpendicular to the chip surface compared to conventional loop inductors.

The idea of electrically large inductors is conceptually explained in Fig. 21.4.2. According to the figure, the loop inductor is split into multiple segments, which are connected by appropriate driving blocks that ensure a phase relation between the currents in the individual coil segments that corresponds to the current distribution of a low-frequency loop coil, see Fig. 21.4.2 (left). In principle, an N-fold segmentation allows for an N-fold increase in the outer perimeter of the coil for a given radiation loss. Fortunately, the required driving blocks can conveniently be realized as cross-coupled VCO cores, resulting in the structure of Fig. 21.4.2 (right).

Thanks to its significantly enlarged diameter, the ac current inside the electrically large inductor produces the required B_1 field in a much larger volume compared to a simple loop coil while keeping losses low. It should be noted that the idea of splitting a coil into multiple segments with intermediate VCO cores was proposed in [3] and extended to higher frequencies (27 GHz) in [4] for the purpose of enhancing the coil's Q-factor. By contrast, here, we make use of the segmented coil technique to design electrically large inductors as sensors for HFEPR and B_1 field sources for high-field EPR/DNP with significantly enlarged active volumes compared to simple loop inductors. Interestingly, in a segmented-coil VCO, the oscillating VCO voltage is accessible at multiple outputs, enabling truly 2D injection-locked VCO arrays, see Fig. 21.4.2 (right). This is in contrast to previously presented injection-locked EPR-on-a-chip detectors [2], where each array element could only be coupled to its two nearest VCO neighbors, resulting in a mostly linear injection scheme. Figure 21.4.2 (right) shows the final layout of the 210 µm x 210 µm 263 GHz 4-segment VCO cell used in this work, including its connection points to its array neighbors. In Fig. 21.4.2 (right), the segmented coil is the central square with a side length of 100 µm, including 4 VCO cores connecting the individual segments. To ensure properly synchronized phases among the VCO cores and to avoid a potential dc-latch and other parasitic oscillation modes [3,4], we have used thin, highly resistive traces bridging the VDD-connected central points of the four coil segments.

Figure 21.4.3 (top) depicts the equivalent circuit model with component values of one VCO cell. To provide sufficient negative conductance by the cross-coupled pairs at the desired frequency of 263 GHz, we have used a capacitive degeneration circuit [5] implemented as large-value tail inductors (L_{tail}) acting as an open in combination with tail capacitors C_{tail} in parallel with the MOS varactors C_{var}. The tail inductors are realized as transmission lines/slab inductors, see Figure 21.4.2 (right). Figure 21.4.3 (bottom) shows the overall architecture of the presented VCO array chip. The array comprises 8x4 segmented-coil VCOs, each injection-locked to its 4 neighboring VCOs using 10 fF coupling capacitors. The joint array frequency is taken from one VCO, minimizing asymmetrical loading effects, then buffered and processed by a divide-by-3 injection-locked frequency divider (ILFD). The input-referred tuning range of the ILFD in the free-running condition was designed 3x larger than that of the VCO array to ensure overlap of the two ranges in all PVT conditions. In the presented prototype chip, the tuning voltage of the ILFD is generated off-chip to provide an extra degree of freedom for the co-tuning of the ILFD and the VCO array. The output frequency of the ILFD is then fed into a regenerative divide-by-2 circuit whose output feeds a chain of CML dividers. The design has two frequency outputs with division factors of 192 and 384, corresponding to output frequencies of 1.37 GHz and 685 MHz, respectively.

The chip was manufactured in a 130 nm BiCMOS technology (f_{max}=450 GHz). It occupies an area of 4.2 mm^2 and has a power consumption of 4.3 W. We have first characterized the chip electrically by measuring its tuning characteristic, see Fig. 21.4.4 (top), confirming a tuning range of more than 2 GHz, which is sufficient to detect most EPR spectra and covers the range of most DNP agents. Next, we proceeded by measuring the phase and frequency noise. The corresponding results, referred to the VCO frequency are shown in Fig. 21.4.4 (bottom left and right). According to the figure, the measured results match well with the worst-case corner simulations (full 3D extraction). Finally, we also performed a preliminary characterization in the target EPR application. To this end, we embedded the chip into a PLL on the PCB level and performed a continuous-wave frequency sweep EPR experiment inside a preclinical 9.4 T MRI scanner. Fig. 21.4.5 (top) shows the measurement setup. The resulting spectrum from a sample of BDPA, a common EPR standard, is shown in Fig. 21.4.5 (bottom). Fig. 21.4.6 compares the presented design against the state-of-the-art (SOTA) in chip-integrated EPR detectors. Compared to the SOTA in chip-integrated HFEPR detectors [1], the presented design achieves a 350x larger sensitive volume and a 4.8x lower frequency noise while operating at a 1.8x higher frequency and providing frequency tunability. A proof-of-concept EPR signal recorded inside a 9.4T MRI scanner validates the proposed approach. Overall, with its increased active volume at high frequencies due to the large channel count and the extended range perpendicular to the chip surface, enabled by the segmented coil design, the presented chip presents a promising alternative for the bulky and costly conventional HFEPR and high-frequency DNP equipment. As an example, compared to a conventional gyrotron, the presented chip produces similar B_1 strengths in the region of interest at a 10^9x reduced size and a 1'000x reduced power consumption while providing frequency agility as required by all modern DNP sequences. Moreover, it does not require additional detection electronics. This can pave the way for the next generation of affordable yet high-performance HFEPR and DNP spectrometers.

Acknowledgement: The authors thank Dominik von Elverfeldt and Lorenzo Tesi for their supports. This work has been supported by the BMBF project EPRoC under contract number 03SF0565A, and the DFG under contract numbers AN 984/25-1 and INST 121384/270-1.

References:

[1] Matheoud, A. V et al., "Single-chip electron spin resonance detectors operating at 50 GHz, 92 GHz, and 146 GHz", *Journal of Magnetic Resonance,* 278, pp. 113-121, 2017.

[2] Anh Chu et al., "An 8-channel 13GHz ESR-on-a-Chip injection-locked VCO-array achieving 200µM-concentration sensitivity," *ISSCC*, pp. 354–355, 2018.

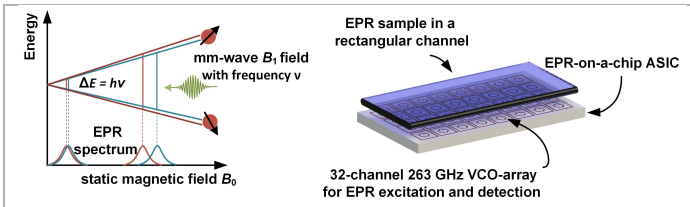

Figure 21.4.1: (Left) EPR principle, (right) 32-channel detector array for EPR measurements.

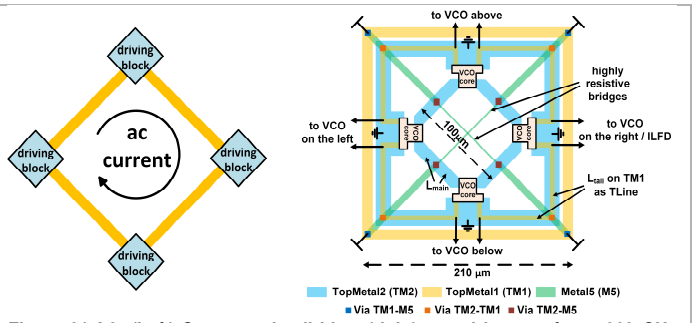

Figure 21.4.2: (Left) Segmented-coil idea, (right) actual layout of one 263 GHz segmented-coil VCO cell.

VCO-array components	Value
L_{main}	16pH, Q=20
C_{ac}	60fF
R_b	5kΩ
C_{tail}	2.8fF
L_{tail}	65pH, Q=6
C_{cpl}	10fF

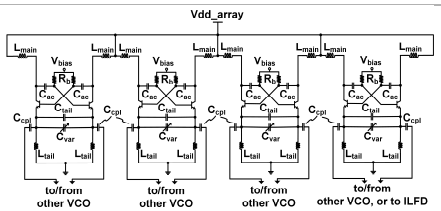

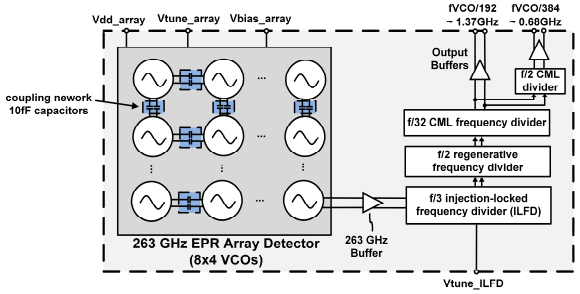

Figure 21.4.3: (Top) equivalent circuit of one 263 GHz segmented-coil VCO cell, (bottom) chip architecture.

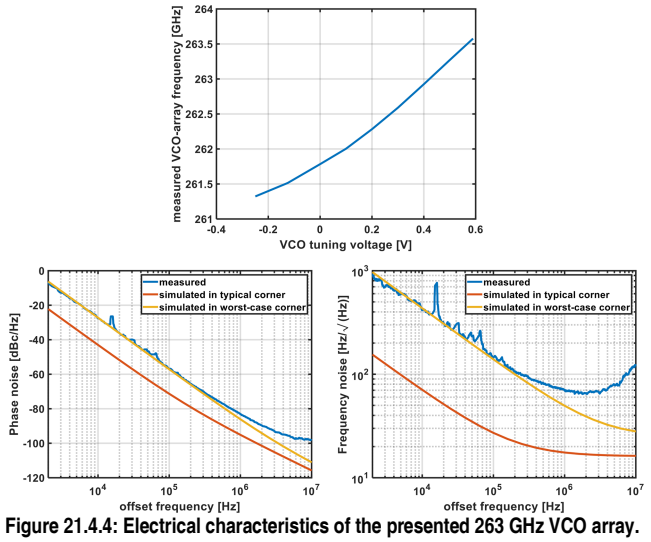

Figure 21.4.4: Electrical characteristics of the presented 263 GHz VCO array.

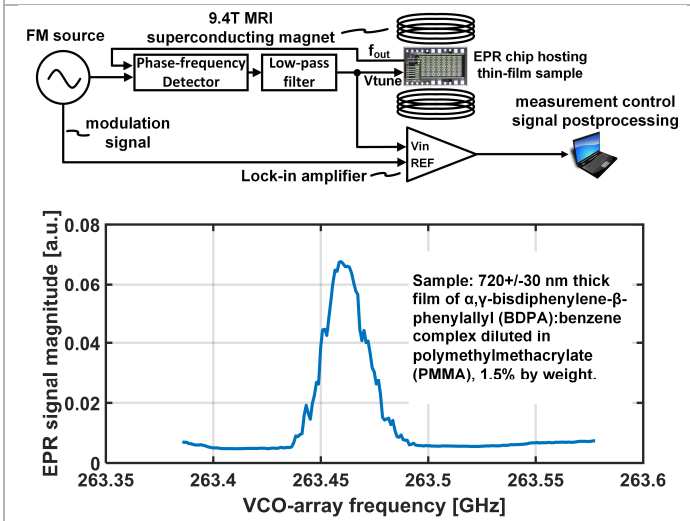

Figure 21.4.5: (Top) EPR measurement setup, (bottom) preliminary EPR spectrum.

	This work	[1] JMR'17	[2] ISSCC'18	[6] ISSCC'16	[7] RSI'08	[8] JMR'12	[9] IMS'13
Field strength [T]	9.4	5.2	0.5	0.5	0.35	0.96	0.034
Operating frequency [GHz]	261.3-263.6	146, fixed frequency	11.8 – 14.2	13.2 – 14.3	9	27	0.77 – 0.97
Sensitive volume	32 nl	0.09 nl	120 nl	27 nl	1 nl	1 nl	External micro resonators of different size
Frequency noise @ 100 kHz offset [Hz/√Hz]	145	700	2	30	10	20	Not specified
ASIC power consumption/ch [mW]	100/ch*	2	15/ch	15	160	75	Not specified
FoM[&] @ 100kHz offset	150.1**	163.4	175.8**	161.6	157	163.9	NA
Complexity of additionally required components	low	high	low	low	high	high	low
Technology	0.13 µm BiCMOS	40 nm CMOS	0.13 µm CMOS	0.13 µm CMOS	0.35 µm CMOS	0.13 µm CMOS	0.13 µm BiCMOS

*power consumption of frequency dividers and buffers not included. Each channel (VCO-cell) consists of 8 transistors biased at ~6 mA from a voltage supply of 2 V.

[&]defined as $\mathrm{FoM} = |\mathrm{PN}| + 20\log_{10}(f_0/\Delta f) - 10\log_{10}(P_{DC}/1\mathrm{mW})$

**calculated from power consumption of the whole array

Figure 21.4.6: Performance summary and comparison with prior arts in IC-based EPR detection.

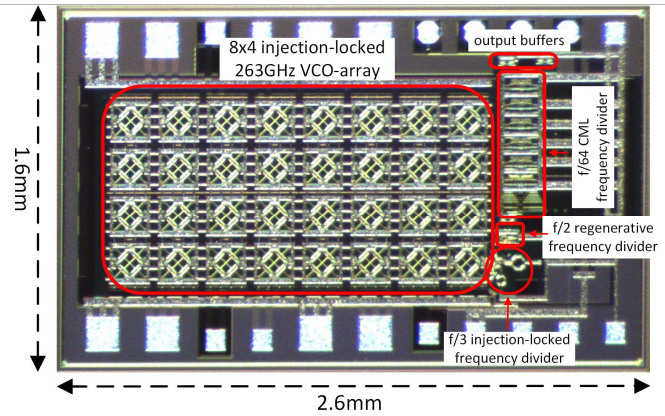

Figure 21.4.7: Chip micrograph.

Additional References:
[3] R. Aparicio and A. Hajimiri, "Circular-geometry oscillators," ISSCC, pp. 378-533, 2004. [4] D. Murphy and H. Darabi, "A 27-GHz Quad-Core CMOS Oscillator With No Mode Ambiguity," IEEE JSSC, vol. 53, no. 11, pp. 3208-3216, 2018. [5] S. Khiyabani et al., "A Compact 275 GHz Harmonic VCO with -2.6 dBm Output Power in a 130 nm SiGe Process," IEEE CICC, pp. 1-4, 2019. [6] J. Handwerker, et al., "A 14GHz Battery-Operated Point-of-Care ESR Spectrometer Based on a 0.13μm CMOS ASIC," ISSCC, pp.476-477, 2016. [7] T. Yalcin, et al., "Single-Chip Detector for Electron Spin Resonance Spectroscopy," Rev. Sci. Instrum., 79(9), pp. 1-6, 2008. [8] J. Anders, et al., "K-Band Single-Chip Electron Spin Resonance Detector," J. Magn. Reson., 217, pp. 19-26, 2012. [9] Y. Xuebei et al., "A Single-Chip Dual-Mode CW/pulse Electron Paramagnetic Resonance Spectrometer in 0.13μm SiGe BiCMOS," Int. Microwave Symp. Dig. Tech. Papers, 2013.